15

Double-mirror monochromator for 4+ generation SKIF synchrotron

© E.I. Glushkov,[1] A.A. Akhsakhalyan,[1] P.A. Veprev,[1] I.G. Zabrodin,[1] M.V. Zorina,[1] I.V. Malyshev,[1] M.S. Mikhailenko,[1] A.E. Pestov,[1] E.V. Petrakov,[1] R.S. Pleshkov,[1] E.S. Antyushin,[1] V.N. Polkovnikov,[1] D.G. Reunov,[1] A.B. Ulasevich,[1] A.K. Tchernyshev,[1] N.I. Chkhalo,[1] R.A. Shaposhnikov,[1] Y.V. Rakshun,[2,3] Yu.V. Khomyakov,[2,4] V.A. Tchernov,[2] I.P. Dolbnya[5]

[1]Institute of Physics of Microstructures, Russian Academy of Sciences,
603950 Nizhny Novgorod, Russia
[2]Budker Institute of Nuclear Physics, Siberian Branch, Russian Academy of Sciences,
630090 Novosibirsk, Russia
[3]Sobolev Institute of Geology and Mineralogy, Siberian Branch Russian Academy of Sciences,
630090 Novosibirsk, Russia
[4]Shared Research Facility „Siberian Circular Photon Source“,
630559 Koltsovo, Novosibirsk, Russia
[5]Dimond, OX11 0DE,
Didcot, UK
e-mail: eglushkov@ipmras.ru

Received June 6, 2025
Revised June 6, 2025
Accepted June 6, 2025

A double-mirror monochromator for an operating photon energy range of 10−30 keV has been developed by the Institute of Physics of Microstructures, Russian Academy of Sciences, for the 4+ generation SKIF synchrotron light source. Multilayer X-ray mirrors were used for synchrotron light monochromatization. Operating range of the device is divided into three subranges: 10−19 keV, 19−30 keV and 19−30 keV with high spectral resolution. To implement such operating mode of monochromator, three multilayer Mo/B_4C, W/B_4C and Cr/Be X-ray mirror strips 6 mm in height each were deposited onto substrates. Depending on the photon energy and subrange, resolution varies within 0.35 %−1.5 %. Mirror reflection coefficients are higher than 60 %. Subrange rearrangement is performed by vertical movement of mirrors. The study describes the principle of operation and design of the device, fabrication techniques used for high-precision substrates, device and components specifications.

Keywords: X-ray optics, synchrotron radiation, double-mirror monochromator, multilayer X-ray mirrors.

DOI: 10.61011/TP.2025.10.62087.125-25

Introduction

It is planned that the 4+ generation SKIF synchrotron radiation (SR) source developed by the Siberian Branch of the Russian Academy of Sciences for Station 1−1 „Mikrofokus“ will use confocal fluorescence microscopy, μ-XANES spectromicroscopy, single-crystal microdiffraction, scanning transmission microscopy and ptychography methods [1–3]. Fourth-generation synchrotrons feature high mean beam power that causes thermally-induced mirror surface and crystal monochromator lattice distortions. This results in the loss of resolution, both spatial and spectral. A double-mirror monochromator (DMM) based on multilayer X-ray mirrors (MXM) was proposed to solve this problem similar to [4–7]. It can fulfil two main functions. In high spectral resolution experiments, it is used for preliminary beam monochromatization, $\Delta E/E \sim 1\,\%$, thus, reducing the crystal-absorbed power by orders of magnitude. For microscopy and elemental microanalysis applications, the monochromator provides a desired increase in test beam intensity due to monochromatization that is 2 to 3 orders of magnitude lower than that of crystals.

A number of complex scientific, engineering and technological problems were solved to implement this device. In particular, to maintain the diffraction quality of reflected wavefronts (for ptychography and nanometer resolution microanalysis), the mirrors shall provide slope errors of reflected wavefronts of 1 μrad and lower, which corresponds to the surface shape accuracy within 1 nm. This problem is complicated by a high SR beam power of 150 W absorbed in the mirror, i.e. the high-precision X-ray mirror surface manufacturing and metrology issues should have been resolved an a mirror compensating thermally-induced surface distortion should have been designed.

Due to a large operating energy range, 10−30 keV, and limited operating angles of mirrors 0.5−0.95° (the reasons for this limitation will be described below), this range might be covered using at least two MXM. Typical spectral resolution of high-reflectivity mirrors is about 1 %, however, for some tasks that are planned at the station, the best resolution is about 0.3 %−0.4 %. Therefore, solutions integrating three pairs of multilayer mirrors in the least expensive way and without opening „to atmosphere“ should have been offered for the monochromator project.

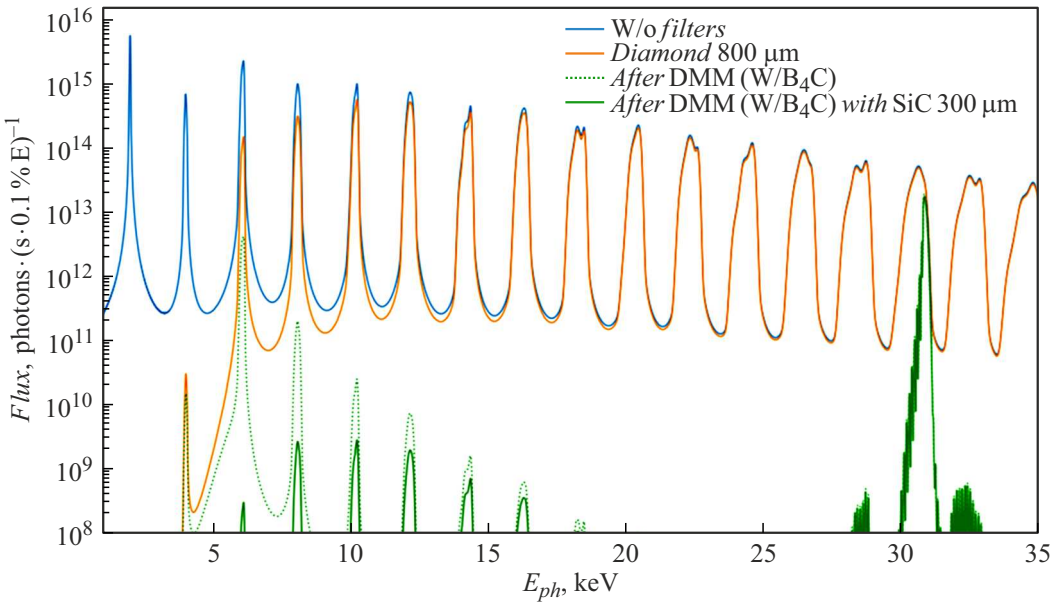

Figure 1. Undulator light spectrum downstream of the frontend, filters and double-mirror multilayer monochromator. The figure as been taken from [2].

In addition, suitable materials and growth process were required to provide so high spectral resolution without sacrificing high reflection coefficients.

This study describes in detail the operating principle and configuration of the device, methods used for producing high-precision substrates and deposition of reflective coatings, water cooling design, and device and components specifications.

1. Light source specifications

A superconducting undulator with the period $\lambda_u = 15.6$ mm, magnetic length $L \approx 2$ m and maximum axial magnetic field $B = 1.25$ T [2] developed by the Institute of Nuclear Physics, Siberian Branch of the Russian Academy of Sciences, will be used to produce radiation at the „Mikrofokus“ station. The fundamental harmonic energy of undulator radiation with a maximum field is 2.06 keV, the fifth (10.3 keV) and fifteenth (30.9 keV) harmonics correspond to the operating range edges. The expected parameters are: rms dimensions of the source $32.9 \times 5.9\,\mu$m, rms radiation divergence at resonance energies of the fifth and fifteenth harmonics — $9.4 \times 11\,\mu$rad and $5 \times 10\,\mu$rad, respectively. Station frontend masks will define the angular aperture of $75 \times 75\,\mu$rad. Radiation spectrum emitted at such solid angle is shown in Figure 1. Full radiation power generated by the undulator (i.e. integral in all directions) is 7.1 kW, from which 0.3 kW is accounted for by the defined aperture. Taking into account diamond filters with a total thickness of 800 μm, radiation power downstream of the frontend is 0.15 kW.

2. X-ray optical configuration of the double-mirror monochromator and component functions

X-ray optical configuration of the monochromator, plan view, is shown in Figure 2. Main monochromator components are: input diaphragm (D) that defines the size of a beam striking the mirror and limits off-axis SR propagation further into the optical path, thus reducing backgrounds and heat load on components: primary MXM M1 and secondary MXM M2. Operating principle is as follows. A polychromatic SR beam strikes the first mirror at the angle θ. In accordance with the Bragg condition, a wavelength λ will be reflected from the mirror:

$$\lambda = 2 \cdot d \cdot \sin\theta, \tag{1}$$

where d is the MXM period. Radiation reflected from M1 strikes identical MXM M2 and is reflected with an offset of 11 mm in the same direction as the primary beam. During scanning along the wavelength, the angles of incidence at both mirrors vary synchronously, whilst mirror M1 remains stationary and the second mirror moves parallel to the incident beam in such a way that the reflected beam falls into the center of the mirror. The maximum angle of incidence (measured from the surface) 0.95° corresponds to the minimum center-to-center distance between the mirrors 315 mm and defines the minimum energy of reflected photons. The maximum center-to-center distance is 630 mm.

The monochromatic beam axis offset of 11 mm with respect to the incident beam makes it possible to separate hard gamma quanta along the incident SR beam axis and to absorb them in the braking radiation trap.

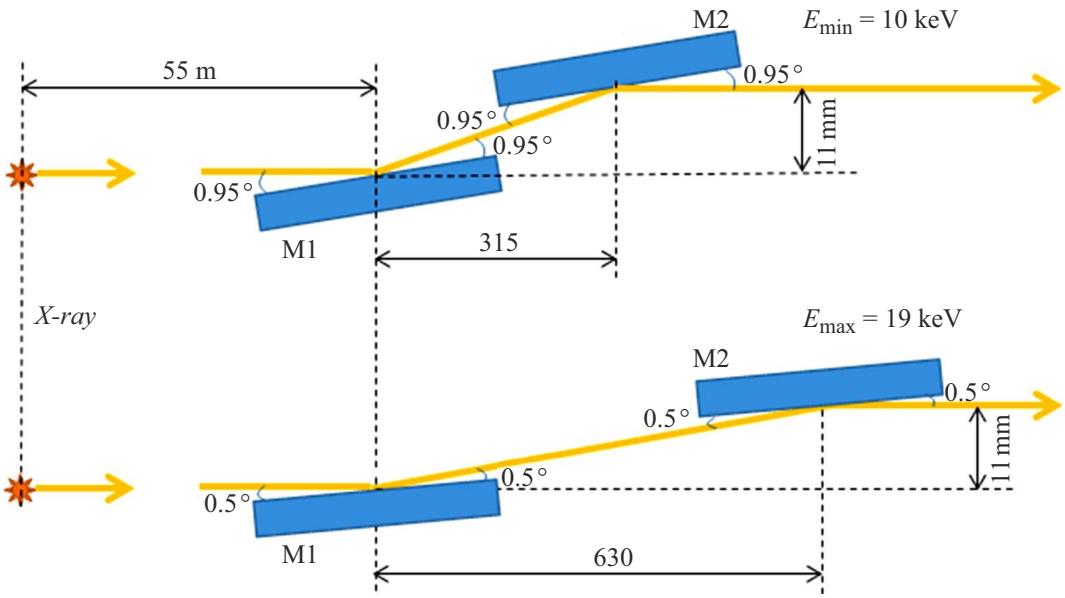

Figure 2. X-ray optical configuration of the monochromator, plan view. Figure: input diagram: M1 and M2 — identical primary and secondary MXMs. Energy data are shown for the first „soft“ subregion.

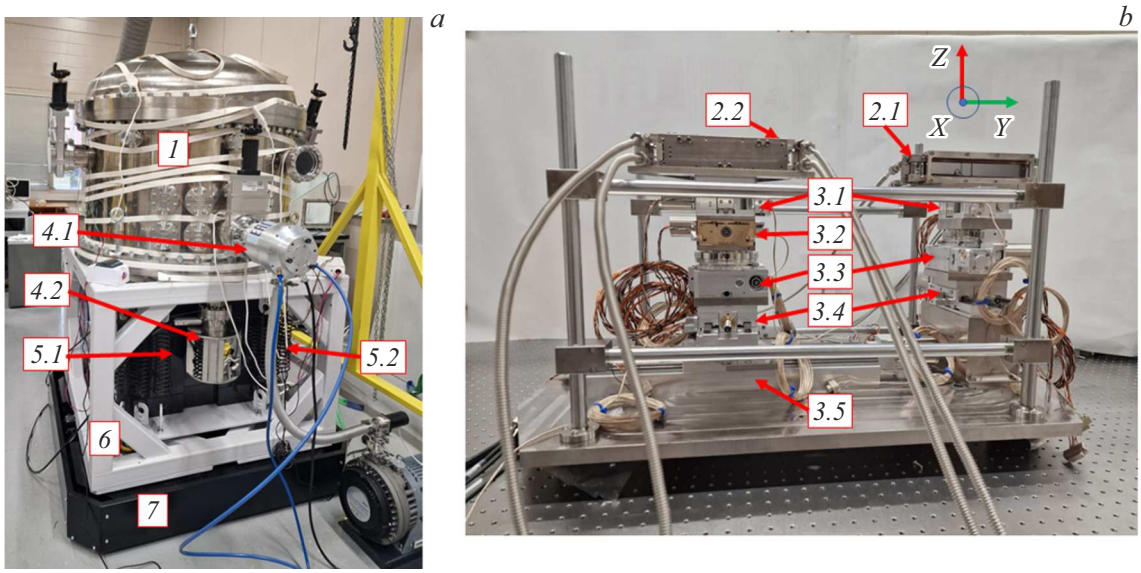

Figure 3. Photograph of the double-mirror monochromator (*a*) and optical-mechanical system placed within the vacuum chamber (*b*). *1* — ultrahigh-vacuum chamber; *2.1* — mirror M1, *2.2* — mirror M2; *3.1* — *Z*-translation stages; *3.2* — *θY* translation stage; *3.3* — *θZ*translation stages; *3.4* — *X* translation stages; *3.5* — *Y* translation stage; *4.1* — turbomolecular pump; *4.2* — Penning-type pumps; *5.1* — gabbro-diabase block; *5.2* — spring hanger; *6* — frame; *7* — 6*D* base.

Figure 3 shows photographs of the double-mirror monochromator and optical-mechanical system placed within the vacuum chamber. Coordinate system is shown in the top right corner. The monochromator consists of the following components: ultrahigh-vacuum chamber *1*, optical-mechanical module (Figure 3, *b*), including two cooled multilayer mirror unit *2* and a set of translation stages: two vertical *3.1*, one tilting stage *3.2*, two rotation stages *3.3*, two linear stages across the beam propagation direction *3.4*, linear stage along the beam propagation *3.5*; turbomolecular pump for preliminary pumping *4.1*; Penning-type pumps, x2 *4.2*; vibration protection module formed by the gabbro-diabase block *5.1* and springs *5.2*; load frame with removed covers *6* and 6*D* mechanical base on vibration dampers *7*.

2.1. Ultrahigh-vacuum chamber

Ultrahigh-vacuum chamber provides high vacuum better than $5 \cdot 10^{-8}$ Torr in the monochromator. The presence of high vacuum avoids X-ray absorption during X-ray trans-

portation from the source to the test sample and minimizes contamination of multilayer mirrors by hydrocarbon decomposition products under the action of ionising radiation. The chamber is furnished with a set of CF-16, CF-40, CF-63, CF-100 and CF-150 flanges for connection to the SR channel and monochromatic beam outlet; vacuum pump and vacuum meter assembly; ultraviolet cleaning windows; connection of high-precision air injection valve and reactive gas supply for mirror cleaning; water and power supply inlet connections. Three bellows inlet connections, on which the optical-mechanical module is mounted, are placed on the bottom of the chamber; thus, the optics is uncoupled from the vacuum chamber and assembled directly on the gabbro-diabase block.

2.2. Optical-mechanical module

The optical-mechanical module is designed for fine tuning and monochromatization of a SR beam striking the device. The optical-mechanical module consists of the following components: multilayer mirrors M1 *2.1*, Figure 3, *b* and M2 *2.2* mounted in strain-free frames and equipped with water cooling system, and a translation stage system for M1 *2.3–2.5* and M2 *2.6–2.10*. Fine tuning of both MXMs to the SR beam in horizontal (X axis) and vertical (Z axis) directions is performed using Linear Stage 5101.20 and Z-Stage 5103.A10, respectively. Vertical translation stages *3.1* also perform transition from one MXM strip to another. Angle of radiation incidence on the mirrors is set using the Goniometer 409 designed for rotation about the Z axis. To ensure parallelism between M1 an M2 during initial alignment and wavelength scanning, the second mirror is outfitted with 1-Circle Segment 5202.60 designed for tilting about the Y axis. Mirror M2 with the above-mentioned translation stages is mounted on the Linear Stage 5101.30 due to which a monochromatic beam reflected from M1 hits the center of M2 during wavelength scanning. Translation stage positioning accuracy is ensured by encoders. The system will be calibrated using the synchrotron. Beam position and intensity during reflection from the monochromator mirrors will be used as feedback.

2.3. Vibration protection module

Vibration protection module is designed to suppress vibrations and consists of a gabbro-diabase block that effectively suppresses low-frequency vibrations and a set of springs for high-frequency vibration isolation. To prevent transverse wiggling of the gabbro-diabase block, rubber shock absorbers are placed under it. Load applied to the shock absorbers is adjusted by spring tension. Thus, the optimum vibration control conditions are provided in each particular case.

2.4. 6*D*- mechanical base

6*D*-mechanical base on vibration dampers is designed for coarse tuning of DMM to a synchrotron beam to provide three linear movements and three rotary movements. Vertical adjustment and adjustment in two angular coordinates are performed using the OV-31M vibration dampers. Transverse movements and rotation about the vertical axis are performed by carriages on rails.

2.5. monochromator evacuation

Two NMD-K-0,3-CF150 Penning-type pumps with an evacuation rate of 230 l/s each are used for monochromator evacuation.

3. Specifications of the double-mirror monochromator components

X-ray monochromatization is performed using a pair of multilayer mirrors with three identical strips deposited onto each of them. MXM were deposited by magnetron sputtering in argon. For details of the MXM systems, sputtering methods and primary characterization, see [8].

The first strip is used within 10–19 keV. A pair of Mo/B_4C materials was chosen as MXM, it is often used for this range due to the absence of molybdenum absorption edges in this range [9,10]. Specifications of the synthesized Mo/B_4C MXM: number of periods $N = 150$, period $d = 36.15$ Å, molybdenum fraction per period $\beta = 0.4$, Mo film roughness $\sigma_{Mo} = 2$ Å and B_4C film roughness $\sigma_{B_4C} = 3$ Å range of grazing angles of incidence $\theta = 0.5 - 0.95°$. Figure 4 shows measured (asterisks) and calculated (lines with symbols) spectral dependences of reflection coefficient R and spectral selectivity $\Delta E/E$ after two reflections. The calculated curve was plotted using the structural parameters of MXM recovered from $R(\theta)$ at 1.54 Å using a method described in [11]. For details of the properties of Mo/B_4C MXM fabricated by the Institute of Physics of Microstructures, Russian Academy of Sciences, including mirrors with ultrashort periods, see [12].

W/B_4C MXM are traditionally used in the subrange of 19–31 keV [13,14]. MXM with the following parameters were deposited in our case: $N = 300$, $d = 21$ Å, $\beta = 0.38$, $\sigma_W = 2.5$ Å, $\sigma_{B_4C} = 4.9$ Å, $\theta = 0.55 - 0.9°$ and Cr/Be $N = 300$, $d = 20$ Å, $\beta = 0.5$, $\sigma_{Cr} = 4.3$ Å, $\sigma_{Be} = 4.3$ Å, $\theta = 0.55 - 0.95°$. Figures 5 and 6 show the corresponding curves. The second strip with Cr/Be MXM is used in this range because of its high spectral resolution, which is required to achieve a number of tasks, including small-angle scattering. Possibility to produce high-reflection Cr/Be MXM with ultrashort periods was demonstrated in [17].

Note that multilayer mirrors are subjected to significant radiation load. Due to cooling, the operating temperature of mirrors is not higher than 30 °C. However, in [12], it is shown that the reflection coefficient of Mo/B_4C coating isn't degraded until 300 °C. W/B_4C coating withstands heating

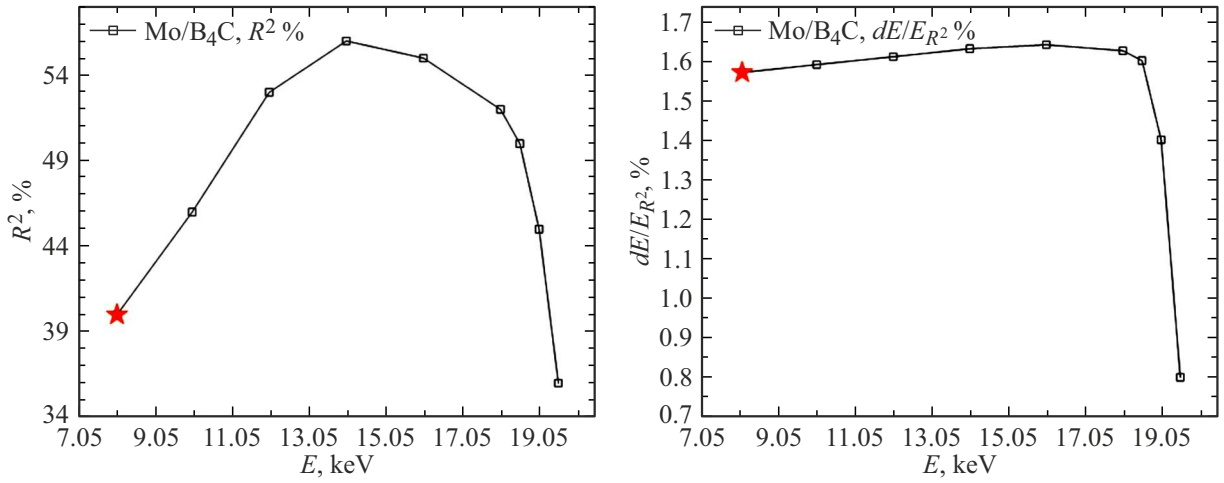

Figure 4. measured (asterisks) and calculated (lines with symbols) spectral dependences of reflection coefficient R and spectral selectivity $\Delta E/E$ after double reflection. Subrange № 1, Mo/B_4C MXM with the following parameters: number of periods $N = 150$, period $d = 36.15$ Å, molybdenum fraction per period $\beta = 0.4$, Mo film roughness $\sigma_{Mo} = 2$ Å and B_4C $\sigma_{B_4C} = 3$ Å.

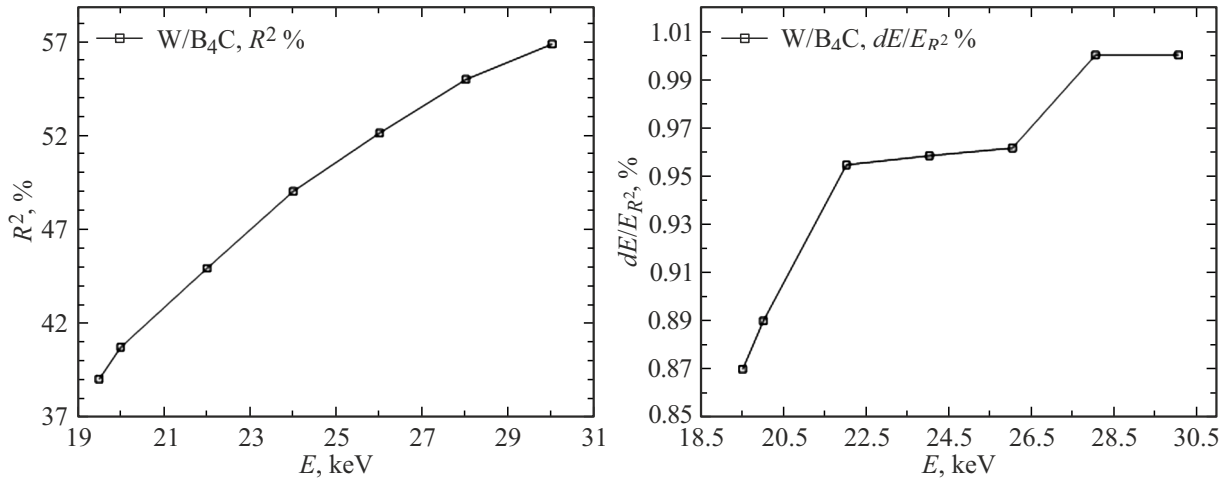

Figure 5. Spectral dependences of reflection coefficient R and spectral selectivity $\Delta E/E$ after double reflection. Subrange № 2, Mo/B_4C MXM with the following parameters: number of periods $N = 300$, period $d = 21$ Å, tungsten fraction per period $\beta = 0.38$, Mo film roughness $\sigma_W = 2.5$ Å and $B_4C_{B_4C} = 4.9$ Å.

to 500 °C [16]. Radiation resistance of Cr/Be hasn't been studied. To remove hydrocarbon decomposition products from mirror surfaces, integration of UV lamps into DMM is planned at the station. These lamps will illuminate the mirrors through sight glasses.

As mentioned above, slope errors of mirrors shall be max. 1 μrad. This condition required, first, high-precision substrate fabrication techniques to be developed, and, second, analysis of thermally-induced reflecting surface distortions in a substrate caused by absorbed SR power > 100 W to be performed. Considering the global experience, single crystal silicon was used as a substrate material [17–19]. Cylindrical workpieces 220 mm in diameter and 25 mm in thickness were used. Fabrication was carried out in several stages. At the first stage, deep grinding and polishing were performed by lapping. The purpose of this stage was to ensure surface flattening in the order of 10 nm. The next stage used chemical and mechanical polishing to achieve effective roughness in the order of 0.2 nm in the spatial frequency range of $0.025-70\,\mu m^{-1}$. For details of the fabrication process and roughness metrology, see [20–22].

At the next stage, water jet cutting method was used to cut out 2002525 mm rectangular workpieces, and longitudinal grooves were made using a milling machine with a diamond tool. Two lower grooves are intended to clamp the mirror in the device using 3 balls. Upper grooves functioned as thermally-induced distortion compensators and will be discussed below. This approach minimizes roughness and high-frequency errors of surface shape.

The final stage of substrate fabrication using a low-size ion beam involved correction of local shape errors: Equipment and correction method are described in [24–29].

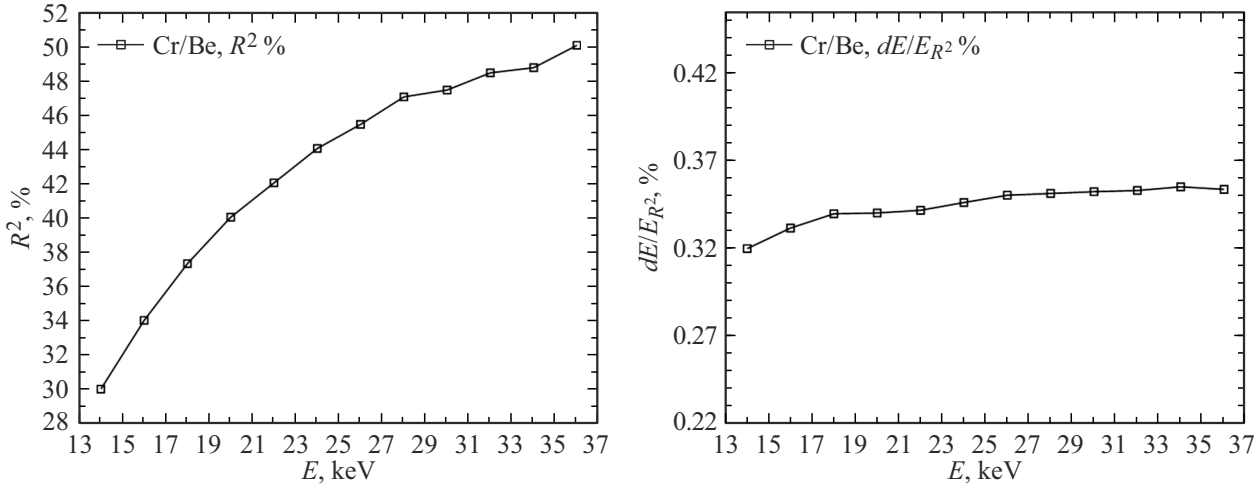

Figure 6. Spectral dependences of reflection coefficient R and spectral selectivity $\Delta E/E$ after double reflection. Subrange № 2, Cr/Be MXM with the following parameters: number of periods $N = 300$, period $d = 20$ Å, chromium fraction per period $\beta = 0.5$, Cr film roughness $\sigma_{Cr} = 4.3$ Å and Be film roughness $\sigma_{Be} = 4.3$ Å.

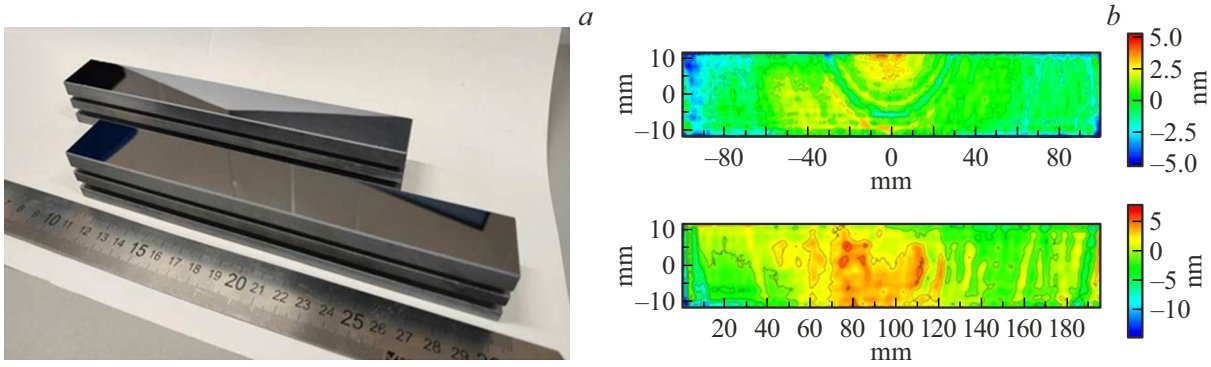

Figure 7. *a* — photograph of mirrors, *b* — error maps of double-mirror monochromator substrates.

Substrate surface shape was measured using the Zygo Verifyer 100 interferometer with a flat reference surface. Large mirror sizes exceeding the interferometer's effective aperture and high shape accuracy in the order of 1 nm required the development of special interference pattern processing methods, consideration of reference surface errors [28–37] and small frame cross-linking of measurements [38–46]. For details of measurement and interference pattern processing methods developed within this work, see [47,48]. Photograph of substrates and error maps are shown in Figure 7.

According to our experience, the described mirror fabrication technique provides X-ray optical components with roughness better than 0.2 nm and shape error better than 2 nm for mirrors longer than 100 mm and accuracy of ± 0.6 nm.

The highest heat load is applied to the Mo/B_4C strip that is deposited in the center of the substrate for effective cooling. W/B_4C and Cr/Be strips are deposited along the substrate edges. Center-to-center distances between the strips were set to 6 mm. The maximum absorbed radiation power was 137 W at the angle of incidence of 0.95°. Substrates are cooled by water flowing via copper coolers attached to a substrate on top with an indium spacer. As shown in a number of studies, this cooling method minimizes thermally-induced shape errors [7,49,50]. Cooling was calculated in SolidWorks Fluent that offers due consideration of cooling fluid velocity and direction. The best parameters were found during the calculation: cooler width — 8 mm, channel diameter — 6 mm, water flow rate — 4 l/min, water inlet temperature — 21 °C. The substrate was cooled on two sides by opposite independent flows.

Thermally-induced surface distortion and distortion and slope error cross-sections, respectively, are shown for a substrate without upper longitudinal grooves in Figure 8, *a*, *c*. As can be seen from the figure, the maximum surface profile height is about 350 nm, and the slope error is in the order of 4 μrad.

To minimize the effect of thermally-induced shape distortions, mirror substrates were fabricated using a „smart-cut“ technique [7,50]. This is a technique where grooves with

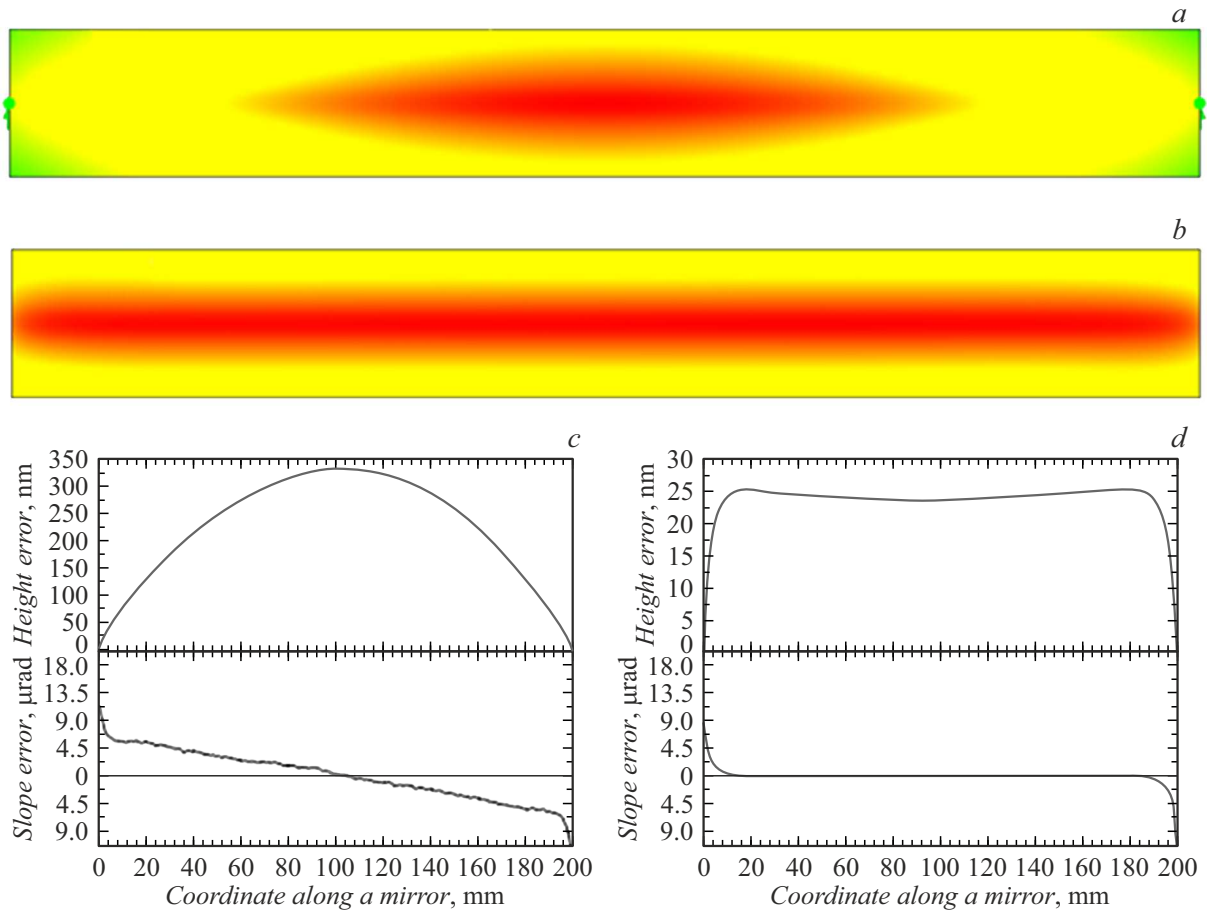

Figure 8. Map of thermally-induced distortion of a silicon substrate without grooves (*a*); central longitudinal cross-section and slope error of silicon without grooves. RMS slope error 3.81 μrad (*c*); map of thermally-induced distortion of a silicon substrate without grooves (*b*); central longitudinal cross-section and slope error of silicon without grooves. RMS slope error 0.26 μrad (*d*).

defined dimensions minimizing the slope error of shape are cut along a substrate. The best groove dimensions were found during the calculation: depth — 3.4 mm, width — 3 mm (Figure 9). As can be seen from Figure 8, *b*, *d*, the longitudinal distortion trace of the beam became more uniform and distortion decreased by almost an order of magnitude. Moreover, if a narrow near-edge region were excluded, then the slope errors were 0.1–0.2 μrad.

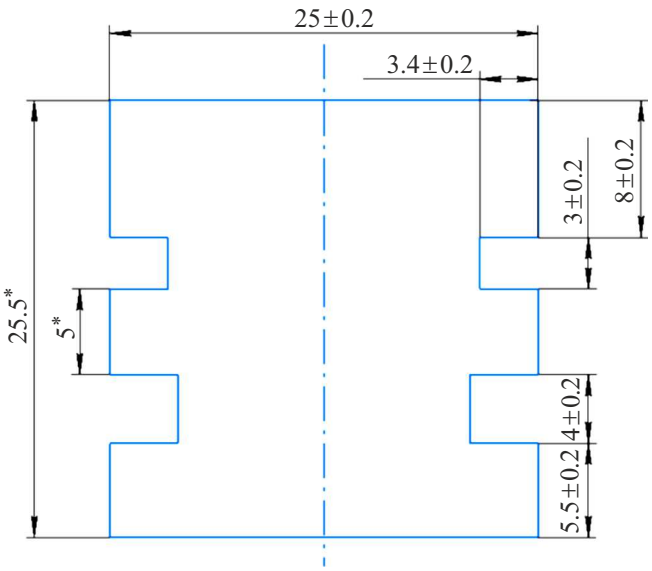

Figure 9. Drawing of DMM with top-cooled substrates. Lower grooves are used to secure the substrate in the frame.

Lower grooves in silicon are used to fix the substrate in the frame using „ball“-to-„ball“ clamping. According to the calculations in SolidWorks, this clamping method ensures RMS shape distortions in the order of 0.1 nm with ball clamping force of 1 kgf.

Final measurements of wavefront slope errors after reflection from the mirrors were carried out on an X-ray optical bench simulating a SR beam. The Microbox microfocus X-ray tube with a focal spot size of 10 μm, power of 7.5 W and copper anode is used as an X-ray source. A Kirkpatrick-Baez system [51–53] with mirrors in the form of platinum-coated parabolic cylinders was used for two-dimensional collimation of radiation emitted by the X-ray tube. To avoid X-ray absorption and scattering in air, the bench has vacuum ducts with polyamide foil windows. Due to this configuration, the detector is moved at a distance more than 5 m from

DMM specifications

Description	Value
Operating range, keV	10−30
Peak double reflection coefficient within 10−19 keV for Mo/B_4C, %	57
Spectral selectivity with double reflection within 10−19 keV for Mo/B_4C, %	1.4−1.6
Peak double reflection coefficient within 19−30 keV for W/B_4C, %	57
Spectral selectivity with double reflection within 19−30 keV for W/B_4C, %	0.87?1
Peak double reflection coefficient within 19−30 keV for Cr/Be, %	50
Spectral selectivity with double reflection within 10−19 keV for Cr/Be, %	0.32−0.35
Angular resolution of energy scanning, μrad	0.9
Mirror substrate cooling	Water cooling
Ultimate vacuum in the vacuum camera, Torr	$5 \cdot 10^{-8}$

the test mirror, thus providing submicroradian sensitivity to wavefront slope errors. For detailed description of the bench, see [54]. X-ray measurements performed on the bench proved all optical interferometry measurements. Thus, the mirrors provided for the double-mirror monochromator ensure reflected wavefront errors in the order of max. 1 μrad. For DMM specifications, see the table.

Conclusion

A double-mirror monochromator for the 4+ generation SKIF synchrotron has been created by the Institute of Physics of Microstructures, Russian Academy of Sciences. The monochromator works in the range of 10−30 keV. SR beam monochromatization is provided by two strip mirror units. Monochromatization within 10−19 keV is provided by Mo/B_4C coating with a peak double reflection coefficient of 57 % and selectivity of 1 %−1.6 %. W/B_4C coatings with a peak double reflection coefficient of 57 % and selectivity of 0.86 %−1 % and a Cr/Be strip with a peak reflection coefficient of 50 % and selectivity of 0.3 %−0.35 % are used within 19−30 keV,

For compensation of thermally-induced distortions, the substrates were made from single crystal silicon using the „smart-cut“ technique with water cooling. The design thermally-induced distortion along the mirror is 0.2 μrad.

Chemical and mechanical polishing and ion-beam machining were used to achieve the effective surface roughness of $\sigma = 0.18$ nm. Substrate shape RMSD is max. 2 nm.

Divergence induced by silicon substrate irregularities and measured using a collimated X-ray beam is less than 1 μrad

Funding

The study was supported by state assignment № FFUF-2024-0022. MXM fabrication and testing were supported by grant of the Russian Science Foundation № 21-72-20108.

Conflict of interest

The authors declare no conflict of interest.

References

[1] Ya.V. Zubavichus. *Tekhnologicheskaya infrastruktura sibirskogo kol'tsevogo istichnika fotonov „SKIF“. Tom 1. Eksperimentalnye stantsii pervoi ocheredi i Laboratorny kompleks* (In-t kataliza im. G.K.Boreskova SO RAN, Novosibirsk, 2022) (in Russian)

[2] Ya.V. Rakshun, Yu.V. Khomyakov, E.I. Glushkov, A.S. Gogolev, M.V. Gorbachev, A.V. Dar'in, F.A. Dar'in, I.P. Dolbnya, S.V. Rashchenko, V.A. Tchernov, N.I. Chkhalo, M.R. Sharafutdinov. Izvestiya TPU. Inzhiniring georesursov, **336** (5), 229 (2022).(in Russian) (2025). DOI: 10.18799/24131830/2025/5/5122

[3] S.V. Rashchenko, M.A. Skamarokha, G.N. Baranov, Y.V. Zubavichus, I.V. Rakshun. AIP Conf. Proceed., **2299** (1), 060001 (2020). DOI: 10.1063/5.0030346

[4] P. Deschamps, P. Engström, S. Fiedler, C. Riekel, S. Wakatsuki, P. Høghøj, E. Ziegler. Synchrotron Radiation, **2** (3), 124 (1995). DOI: 10.1107/S0909049595001592

[5] T. Koyama, Ya. Senba, H. Yamazaki, T. Takeyuchi, M. Tanaka, Ya. Shimizu, K. Tsubota, Ya. Matsuzaki, H. Kishimoto, T. Miura, S. Shimizu, T. Saito, H. Yumoto, K. Uesugi, M. Hoshino, J. Yamada, T. Osaka, M. Sugahara, N. Nariyama, Ya. Ishizawa, H. Nakano, C. Saji, Kyo Nakajima, K. Motomura, Ya. Joti, M. Yabashi, H. Ohashi. Synchrotron Radiation, **29** (5), 1265 (2022).
DOI: 10.1107/S1600577522006610

[6] K.J.S. Sawhney, I.P. Dolbnya, S.M. Scott, M.K. Tiwari, G.M. Preece, S.G. Alcock, A.W. Malandain. In: *Advances in X-Ray/EUV Optics and Components VI*, **813908** (SPIE, 2011), p. 79−86. DOI: 10.1117/12.894920
[7] P. Brumund, J. Reyes-Herrera, C. Morawe, T. Dufrane, H. Isern, T. Brochard, M. Sánchez del Río, C. Detlefs. J. Synchrotron Radiation, **28**, 1423 (2021). DOI: 10.1107/S160057752100758X
[8] A.D. Akhsakhalyan, E.B. Klyuenkov, A.Ya. Lopatin, V.I. Luchin, A.N. Nechai, A.E. Pestov, V.N. Polkovnikov, N.N. Salashchenko, M.V. Svechnikov, M.N. Toropov, N.N. Tsybin, N.I. Chkhalo, A.V. Shcherbakov. Poverkhnost'. Rentgenovskie, sinhrotronnye i neitronnye issledovaniya **1**, 5 (2017) (in Russian). DOI: 10.7868/S0207352817010048
[9] D.-G Liu, C.-H. Chang, C.-Y. Liu, S.-H. Chang, J.-M. Juang, Y.-F. Song, K.-L. Yu, K.-F. Liao, C.-S. Hwang, H.-S. Fung, P.-C. Tseng, C.-Y. Huang, L.-J. Huang, S.-C. Chung, M.-T. Tang, K.-L. Tsang, Y.-S. Huang, C.-K. Kuan, Y.-C. Liu, K.S. Liang, U.-S. Jeng. J. Synchrotron Radiation, **16**, 97 (2009). DOI: 10.1107/S0909049508034134
[10] M.A. Blokhin, I.G. Shveitser. *Rentgenospekralny spravochnik* (Nauka, M, 1982) (in Russian)
[11] M. Svechnikov. J. Appl. Crystallogr., **53** (1), 244 (2020). DOI: 10.1107/S160057671901584X
[12] R. Shaposhnikov, V. Polkovnikov, S. Garakhin, Y. Vainer, N. Chkhalo, R. Smertin, K. Durov, E. Glushkov, S. Yakunin, M. Borisov. J. Synchrotron Radiation, **31** (2), 268 (2024). DOI: 10.1107/S1600577524000419
[13] C.C. Walton. *PhD thesis* (University of California, Berkeley, USA, 1997)
[14] P.C. Pradhan, A. Majhi, M. Nayak. J. Appl. Phys., **123**, 095302 (2018). DOI: 10.1063/1.5018266
[15] A. Rack, Ch. Morawe, L. Mancini, D. Dreossi, D.Y. Parkinson, A.A. MacDowell, F. Siewert, T. Rack, T. Holz, M. Krämer, R. Dietsch. In: *Advances in X-Ray/EUV Optics and Components IX*, **92070V** (SPIE, 2014), p. 213−219. DOI: 10.1117/12.2060801
[16] R. Pleshkov, N. Chkhalo, V. Polkovnikov, M. Svechnikov, M. Zorina. J. Appl. Crystallogr., **54** (6), 1747 (2021). DOI: 10.1107/S160057672101027X
[17] B. Huang, W. Le, Y. Wang, X. Luo, Y. Yang. Appl. Surf. Sci., **464**, 10 (2019). DOI: 10.1016/j.apsusc.2018.09.077
[18] W.K. Lee, K. Fezzaa, P. Fernandez, G. Tajiri, D.M. Mills. Synchrotron Radiation, **8** (1), 22 (2001). DOI: 10.1107/S0909049500013868
[19] H. Thiess, H. Lasser, F. Siewert. Nuclear Instruments and Methods in Physics Research Section A: Accelerators, Spectrometers, Detectors and Associated Equipment, **616** (2−3), 157 (2010). DOI: 10.1016/j.nima.2009.10.077
[20] A. Erko, M. Idir, Th. Krist, A.G. Michette. *Modern Developments in X-ray and Neutron Optics*. (Springer, NY., Berlin, Heidelberg, 2008)
[21] N.I. Chkhalo, I.V. Malyshev, A.E. Pestov, V.N. Polkovnikov, N.N. Salashchenko, M.N. Toropov. UFN, **190** (1), 74 (2020) (in Russian).
[22] U. Dinger, F. Eisert, H. Lasser, M. Mayer, A. Seifert, G. Seitz, S. Stacklies, F. Stickel, M. Weiser. In: Soft X-Ray and EUV Imaging Systems. **4146**, 35−46 (SPIE, 2000). DOI: 10.1117/12.406674
[23] E. Ziegler, L. Peverini, N. Vaxelaire, A. Cordon-Rodriguez, A.V. Rommeveaux, I.V. Kozhevnikov, J. Susini. Nuclear Instruments & Methods in Physics Research Section A-accelerators Spectrometers Detectors and Associated Equipment, **616** (2−3), 188 (2010). DOI: 10.1016/j.nima.2009.12.062
[24] A. Chernyshev, N. Chkhalo, I. Malyshev, M. Mikhailenko, A. Pestov, R. Pleshkov, R. Smertin, M. Svechnikov, M. Toropov. Precision Engineer., **69**, 29 (2021). DOI: 10.1016/j.precisioneng.2021.01.006
[25] S.R. Wilson, D.W. Reicher, J.R. McNeil. In: *Advances in Fabrication and Metrology for Optics and Large Optics*, **996**, 74 (SPIE, 1989). DOI: 10.1117/12.948051
[26] T.W. Drueding, S.C. Fawcett, SR. Wilson, T.G. Bifano. Opt. Engineer., **34** (12), 3565 (1995). DOI: 10.1117/12.215648
[27] M. Xu, Y. Dai, X. Xie, L. Zhou, W. Liao. Appl. Opt., **54** (27), 8055 (2015). DOI: 10.1364/AO.54.008055
[28] M. Zeuner, S. Kiontke. Opt. Photonik, **7** (2), 56 (2012). DOI: 10.1002/opph.201290051
[29] T. Franz, T. Hänsel. In: *Optical fabrication and testing*. OThC7 (Optica Publishing Group, 2008), DOI: 10.1364/OFT.2008.OThC7
[30] B.S. Fritz. Opt. Engineer., **23** (4), 379 (1984). DOI: 10.1117/12.7973304
[31] G. Zhou, W. Lei, X. Dong, J. Wang. Laser Optoelectron. Progress, **60** (23), 2312001 (2023). DOI: 10.3788/LOP222992
[32] G. Zhou, J. Wang, W. Lei, X. Dong, J. Wang. Appl. Opt., **63** (8), 2086 (2024). DOI: 10.1364/AO.516190
[33] U. Griesmann. Appl. Opt., **45** (23), 5856 (2006). DOI: 10.1364/AO.45.005856
[34] I. Powell, E. Goulet. Appl. Opt., **37** (13), 2579 (1998). DOI: 10.1364/AO.37.002579
[35] P.B. Keenan. Pseudo-shear interferometry. In: *Precision Surface Metrology*, **429**, 2−7 (SPIE, 1983). DOI: 10.1117/12.936333
[36] Y.C. Chen, C.W. Liang, H.S. Chang, P.C. Lin. Opt. Express, **26** (22), 29123 (2018). DOI: 10.1364/OE.26.029123
[37] A. Kochetkov, A. Shaykin, I. Yakovlev, E. Khazanov, A. Cheplakov, B. Wang, Y. Jin, S. Liu, J. Shao. Opt. Express, **33** (6), 13673 (2025). DOI: 10.1364/OE.551097
[38] M. Otsubo, K. Okada, J. Tsujiuchi. Opt. Engineer., **33** (2), 608 (1994). DOI: 10.1117/12.152248
[39] M.B. Da Silva, S.G. Alcock, I.T. Nistea, K. Sawhney. Opt. Lasers Engineer., **161**, 107192 (2023). DOI: 10.1016/j.optlaseng.2022.107192
[40] L. Huang, J. Xue, B. Gao, M. Idir. Opt. Express, **26** (8), 9882 (2018). DOI: 10.1364/oe.26.009882
[41] H. Yumoto, T. Koyama, S. Matsuyama, K. Yamauchi, H. Ohashi. Rev. Scientific Instruments, **87** (5), (2016). DOI: 10.1063/1.4950714
[42] P. Murphy, J. Fleig, G. Forbes, D. Miladinovic, G. DeVries, S. O'Donohue. In: *Interferometry XIII: Applications*, **6293**, 150−159 (SPIE, 2006). DOI: 10.1117/12.680473
[43] C. Supranowitz, J.P. Lormeau, C. Maloney, P. Murphy, P. Dumas. In: *Optics and Measurement International Conference 2016*, **10151**, 81−92 (SPIE, 2016). DOI: 10.1117/12.2257279
[44] P. Zhang, H. Zhao, X. Zhou, J. Li. Opt. Express, **18** (14), 15216 (2010). DOI: 10.1364/OE.18.015216
[45] M. Bray. In: *Optical Fabrication and Testing*, **3739**, 259−273 (SPIE, 1999). DOI: 10.1117/12.360153

[46] J. Fleig, P. Dumas, P.E. Murphy, G.W. Forbes. In: *Advanced Characterization Techniques for Optics, Semiconductors, and Nanotechnologies*, **5188**, 296–307 (SPIE, 2003). DOI: 10.1117/12.506254
[47] E.V. Petrakov, N.I. Chkhalo, A.K. Chernyshev, E.I. Glushkov. Opt. Engineer., **63** (11), 114104–1 (2024). DOI: 10.1117/1.OE.63.11.114104
[48] E.V. Petrakov, E.I. Glushkov, A.K. Chernyshev, N.I. Chkhalo. J. Surf. Investigation. X-Ray, Synchrotron and Neutron Techniques, **18** (Suppl 1), S58 (2024). DOI: 10.1134/S1027451024701878
[49] L. Zhang, R. Barrett, K. Friedrich, P. Glatzel, T. Mairs, P. Marion, G. Monaco, C. Morawe, T. Weng. J. Phys.: Conf. Ser., **425** (5), 052029 (2013). DOI: 10.1088/1742-6596/425/5/052029
[50] E.I. Glushkov, I.V. Malyshev, E.V. Petrakov, N.I. Chkhalo, Yu.V. Khomyakov, Ya.V. Rakshun, V.A. Chernov, I.P. Dolbnya. J. Surf. Investigation: X-ray, Synchrotron and Neutron Techniques, **17** (Suppl 1), S233 (2023). DOI: 10.1134/S1027451023070133
[51] P. Kirkpatric, A.V. Baez. J. Opt. Society America, **38** (9), 766 (1948). DOI: 10.1364/JOSA.38.000766
[52] P.J. Eng, M. Newville, M.L. Rivers, S.R. Sutton. In: *X-Ray Microfocusing: Applications and Techniques*, **3449**, 145–156 (SPIE, 1998). DOI: 10.1117/12.330342
[53] Y.S. Uchida. Jpn. J. Appl. Phys., **30** (5R), 1127 (1991). DOI: 10.1143/JJAP.30.1127
[54] D.G. Reunov, A.D. Akhsakhalyan, E.I. Glushkov, I.G. Zabrodin, I.V. Malyshev, M.S. Mikhailenko, E.V. Petrakov, A.K. Chernyshev, N.I. Chkhalo. J. Surf. Investigation. X-Ray, Synchrotron and Neutron Techniques, **18** (Suppl 1), S38 (2024). DOI: 10.1134/S1027451024701842

Translated by E.Ilinskaya